The Journal of Chemical Physics

Structure of two-dimensional Fe_3O_4

Cite as: J. Chem. Phys. **152**, 114705 (2020); https://doi.org/10.1063/1.5142558
Submitted: 14 December 2019 . Accepted: 02 March 2020 . Published Online: 17 March 2020

Lindsay R. Merte, Pär A. T. Olsson, Mikhail Shipilin, Johan Gustafson, Florian Bertram, Chu Zhang, Henrik Grönbeck, and Edvin Lundgren

The Journal of Chemical Physics ARTICLE scitation.org/journal/jcp

Structure of two-dimensional Fe_3O_4

Cite as: J. Chem. Phys. 152, 114705 (2020); doi: 10.1063/1.5142558
Submitted: 14 December 2019 • Accepted: 2 March 2020 •
Published Online: 17 March 2020

Lindsay R. Merte,[1,a)] Pär A. T. Olsson,[1,2] Mikhail Shipilin,[3] Johan Gustafson,[4] Florian Bertram,[5] Chu Zhang,[4] Henrik Grönbeck,[6] and Edvin Lundgren[4]

AFFILIATIONS

[1]Materials Science and Applied Mathematics, Malmö University, 20506 Malmö, Sweden
[2]Division of Mechanics, Lund University, 22100 Lund, Sweden
[3]Department of Physics, Stockholm University, AlbaNova University Center, 10691 Stockholm, Sweden
[4]Division of Synchrotron Radiation Research, Lund University, 22100 Lund, Sweden
[5]DESY Photon Science, Notkestr. 85, 22607 Hamburg, Germany
[6]Department of Physics and Competence Centre for Catalysis, Chalmers University of Technology, 41296 Göteborg, Sweden

Note: This article is part of the JCP Special Topic on Oxide Chemistry and Catalysis.
[a)]**Author to whom correspondence should be addressed:** lindsay.merte@mau.se

ABSTRACT

We have investigated the structure of an ultrathin iron oxide phase grown on Ag(100) using surface x-ray diffraction in combination with Hubbard-corrected density functional theory (DFT+U) calculations. The film exhibits a novel structure composed of one close-packed layer of octahedrally coordinated Fe^{2+} sandwiched between two close-packed layers of tetrahedrally coordinated Fe^{3+} and an overall stoichiometry of Fe_3O_4. As the structure is distinct from bulk iron oxide phases and the coupling with the silver substrate is weak, we propose that the phase should be classified as a metastable two-dimensional oxide. The chemical and physical properties are potentially interesting, thanks to the predicted charge ordering between atomic layers, and analogy with bulk ferrite spinels suggests the possibility of synthesis of a whole class of two-dimensional ternary oxides with varying electronic, optical, and chemical properties.

I. INTRODUCTION

Due to their abundance, low cost, and relatively low environmental impact, iron oxides are attractive materials for implementation in optical, electronic, and magnetic applications, which presently rely heavily upon rare, expensive, and/or toxic elements.[1,2] Although among the oldest functional materials known, the production of iron oxides with nanoscale dimensions—and consequent novel properties—creates opportunities for applications in new areas. Nanoscale iron oxides have shown promise for use in supercapacitors[3] and lithium-ion batteries,[4] biomedical applications and catalysts,[5] and magnetic devices,[6] for example.

The reduction in dimension to the nanoscale gives increasing importance to iron oxide surfaces in determining material properties, and recent studies have begun to provide a detailed atomistic picture of these surfaces.[7] The effects of reduced coordination environment, relaxation, and accommodation of potential non-stoichiometry combine to yield surfaces whose properties may differ substantially from those encountered in the bulk. When thickness is reduced to the atomic scale, the "bulk" of the material is eliminated, and the films must be considered distinct phases with their own properties.[8–10] Interest in 2D materials has increased recently,[11] and a wide variety of materials, including many metal oxides,[12] have been produced in ultra-thin form, usually by exfoliation of layered bulk materials. Especially where 2D materials are formed from compounds that are not inherently layered in the bulk (including the iron oxides, of which a 2D phase produced by exfoliation was recently reported[13]), it is of considerable importance to understand how the drastic change in bonding environments at reduced dimensions affects the structure as well as the chemical and physical properties.

Monolayer FeO films have been studied for decades,[14–17] and although they show a superficial resemblance to rocksalt-structured FeO(111), it has become clear that the monolayer is a distinct phase whose properties cannot be explained by reference to the bulk-terminated FeO surface. FeO monolayers on platinum are

stabilized by relatively strong film–substrate interactions, modifying their properties substantially. The most prominent result of this stabilization is the possibility for the so-called coordinatively unsaturated ferrous (CUF) sites occurring at the edges of FeO islands, which have been shown to activate O_2 in catalytic oxidation reactions.[18–21] The reversible intercalation of oxygen to form an FeO_2 trilayer phase[22,23] is a further manifestation of this. In contrast, FeO grown on silver surfaces, where film–substrate interactions are significantly weaker, shows characteristics different from Pt-supported films and from bulklike FeO(111), instead resembling those of the truly two-dimensional unsupported phase.[24]

Previous experiments[25,26] studying the growth of iron oxides on silver surfaces identified an additional ultrathin phase forming under conditions with higher O_2 pressures, which has somewhat puzzling characteristics: although exhibiting a surface structure similar to FeO(111) and to monolayer and multilayer FeO films grown on a variety of metal substrates previously,[15,26–30] core level spectroscopies indicate instead a mixed-valence compound incorporating both Fe^{2+} and Fe^{3+}. It was proposed[26] that a thin (111)-oriented section of rocksalt FeO composed of three close-packed Fe layers and four close-packed O layers—giving an overall composition of Fe_3O_4—could explain the observations. The presence of a large proportion of Fe^{3+} and the (presumed) absence of a net electrostatic dipole in such a structure suggest that its electronic and chemical properties should differ substantially from those of bulk-terminated FeO(111), magnetite Fe_3O_4, or monolayer FeO.

In this contribution, we report the results of a combined surface x-ray diffraction (SXRD) and density functional theory (DFT) study aimed at determining the structure of this phase. Our results confirm that the structure is based on close-packed Fe and O layers and show that it is not derived from rocksalt FeO. Instead of the pure octahedral stacking seen in the rocksalt phase, the Fe_3O_4 nanosheets are composed of one central layer of octahedral Fe and two outer layers of tetrahedral Fe.

II. METHODS

A. Experiments

STM measurements were performed in ultra-high vacuum at room temperature using an Omicron STM-1 microscope at the Department of Physics, Lund University. XPS and NEXAFS spectra were acquired at beamline I311 at the MAX-II synchrotron, MAX IV Laboratory, Lund. For details of these experiments, see Ref. 26.

SXRD measurements were performed at beamline I07 at the Diamond Light Source using an ultra-high vacuum system installed at Experimental Hutch 2.[31] The Fe_3O_4 sheets were grown, following a procedure established previously,[26] by the deposition of iron from an electron-beam evaporator in a background pressure of 1×10^{-5} mbar O_2, followed by vacuum annealing at 400 °C. The structure was checked by LEED and STM prior to XRD measurements, which were performed in a directly attached chamber of the UHV system. In-plane and out-of-plane XRD scans were made using a Pilatus 100 K area detector and a fixed incident angle of 0.2°. To obtain intensities for the diffraction rods, we performed θ scans with the detector fixed for a series of out-of-plane angles. The collected stacks of images represent a 3D map of the reciprocal space, from which 2D slices through the rods at different L values were extracted. Intensities were extracted by 2D peak fitting of these slices, which allowed separation of intensity corresponding to the diffraction rod from the background.[32] Raw intensities were converted to structure factors after the application of the appropriate Lorentz and polarization corrections.[33] X-ray structure factors for model structures were computed directly in the kinematic approximation (after the work of Vlieg[34]), taking into account the symmetry of the substrate, which results in mirrored domains with overlapping diffraction rods. The slight undulation of the film caused by moiré coincidence was neglected here, as its main influence is expected to be a somewhat increased Debye–Waller parameter. For fits based on DFT structural data, only the overall intensity and Debye–Waller factor were varied.

B. Density functional theory modeling

The DFT+U modeling was conducted using the Vienna *ab initio* simulation package (VASP).[35–38] To describe the electron–ion interaction, we adopted the projector augmented wave (PAW) method[39,40] (PAW, electronic valence configurations: $2s^2 2p^4$, $3p^6 3d^7 4s^1$, $3p^6 3d^7 4s^2$, $3p^6 3d^8 4s^2$, and $4p^6 4d^{10} 5s^1$ for O, Fe, Co, Ni, and Ag, respectively) with the exchange-correlation functional approximated within the Perdew, Burke, and Ernzerhof (PBE) formalism.[41] For calculations of adhesion energies, the Grimme-D2 method[42] was used to include an estimate of van der Waals interactions. To account for the magnetic properties and the strong electronic correlation of the Fe/Co/Ni *d*-states, we utilized a collinear spin modeling approach in tandem with the rotationally invariant Hubbard correction approach suggested in Ref. 43. The effective Hubbard parameters for Fe and Co, $U_{eff} = U - J$, were chosen to be 4.2 eV and 4.0 eV, respectively. With these choices, the gaps between highest occupied and lowest unoccupied 3*d* states match the experimental bandgaps of the bulk rocksalt phases.[44,45] For Ni, the effective Hubbard parameter was chosen as 4.6 eV, in accordance with reported data in the literature.[46]

The electronic Kohn–Sham orbitals were expanded in plane waves and the reciprocal space was discretized by means of a Γ-centered *k*-point grid generated using the Monkhorst–Pack method.[47] The cutoff kinetic energy and *k*-point grid size were converged with respect to the ground state energy of the stoichiometric bulk FeO rocksalt. Thus, it was represented by a hexagonal supercell as in Ref. 46 such that an anti-ferromagnetic type II spin variation along the [111]-direction could be obtained. It was found that a plane wave cutoff of 650 eV and *k*-point grid of $12 \times 12 \times 3$ resulted in a total energy convergence better than 5 meV/FeO-unit.

For modeling the free-standing and supported films, the same parameters as for the rocksalt bulk phase were used except that a planar *k*-point mesh commensurate with that of the hexagonal cell was utilized along with dipole correction to reduce periodic artifacts emanating from dipole interaction across the periodic cell boundary.[48] To further ensure that the films were not affected by the periodicity, we studied how the ground state energy varied with the out-of-plane vacuum dimension. The results showed that a vacuum of 6 Å or larger yielded a convergence accuracy of 1 meV/Fe_3O_4-unit. Hence, we made sure that it was larger than 8 Å in our simulations. For the charge segregation studies, we performed Bader charge analyses[49] using the open-source software BADER.[50]

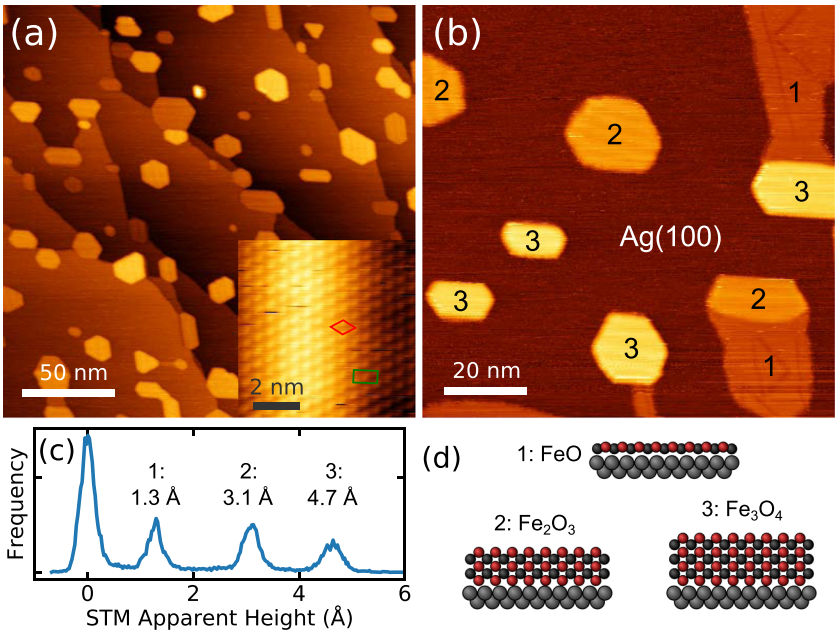

FIG. 1. (a) Large-scale and atomic resolution STM images of multilayer FeO_x grown on Ag(100) in 5×10^{-6} mbar O_2. Hexagonal and centered-rectangular unit cells are marked in the atomic-scale image and correspond to the reciprocal-space cells in Fig. 3. (b) STM image of FeO_x islands on Ag(100) after Fe deposition in 1×10^{-6} mbar O_2 followed by annealing. (c) Height histogram from image (b) showing the apparent heights of the three types of islands imaged. These are interpreted as incorporating one, two, or three close-packed Fe layers and are assigned to FeO, Fe_2O_3, and Fe_3O_4, respectively. (d) Schematic models of the three structures. Data originally reported in Ref. 26.

III. RESULTS

A. Experimental characterization

As discussed previously,[26] deposition of iron onto Ag(100) in a sufficiently low background pressure of O_2 (2×10^{-7} mbar) followed by UHV annealing results in the formation of an FeO monolayer with a hexagonal, boron nitride type structure with a mean Fe–Fe spacing of about 3 Å. When higher oxygen pressures are used or when the FeO monolayer is oxidized and annealed, a new type of structure is formed, which exhibits a similar in-plane periodicity, but is thicker than the monolayer. Figure 1(a) shows islands of this new multilayer phase prepared by depositing in 5×10^{-6} mbar O_2 followed by annealing at 400 °C. The phase consists of hexagonal islands with a wavy height profile due to the moiré-type coincidence of the 3.1 Å lattice parameter with the underlying Ag(100) substrate.

Figure 1(b) shows an STM image of FeO_x/Ag(100) prepared using an intermediate O_2 pressure (1×10^{-6} mbar) where monolayer FeO coexists with islands of the new structure, and an extracted height histogram from this image is shown in Fig. 1(c). Aside from the monolayer at 1.3 Å, two different apparent heights are observed at 3.1 Å and 4.7 Å. These are assigned to structures incorporating 2 and 3 Fe layers, respectively, as well as an additional oxygen layer, to give overall compositions of Fe_2O_3 and Fe_3O_4, as indicated schematically in Fig. 1(d). Due to embedding of islands in the silver surface, whose steps become quite mobile at the temperatures used for annealing, we could not determine directly the distribution of 2-layer and 3-layer islands in the preparation shown in Fig. 1(a), but based on the approximate threefold reduction in the area fraction of the film relative to the monolayer, the 3-layer Fe_3O_4 structure appears predominant. As will be discussed below, SXRD measurements are consistent with a 3-layer structure, with likely contributions of the 2-layer structure as a minority phase. XPS and XAS measurements of the FeO monolayer and multilayer structures, prepared similarly as those characterized by STM, but subjected to post-annealing at a higher temperature of 600 °C, are shown in Fig. 2 together with the corresponding LEED patterns. The spectra (also discussed previously[26]) indicate a combination of Fe^{2+} and Fe^{3+}, consistent with the proposed Fe_3O_4 composition.

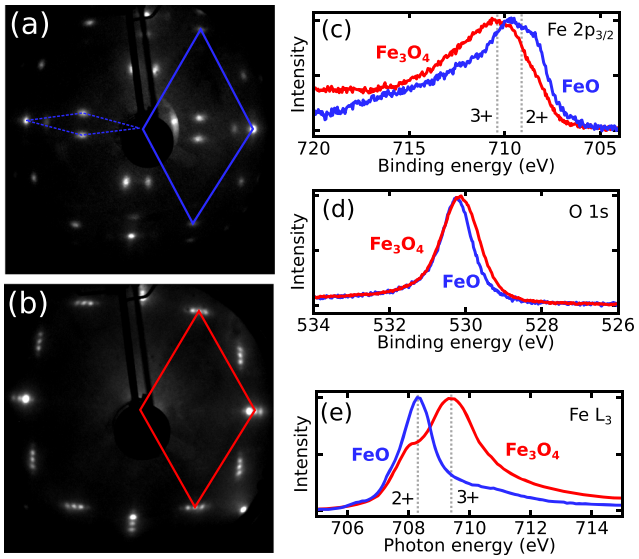

FIG. 2. LEED patterns of (a) monolayer FeO and (b) the Fe_3O_4 multilayer phase as characterized by XPS/XAS. Both indicate a ~3 Å hexagonal lattice (large diamonds) and characteristic reflections due to the moiré coincidence structures. (c) Fe 2p XPS, (d) Fe-L_3 NEXAFS, and (e) O 1s XPS spectra for the two surfaces. Data originally reported in Ref. 26.

To gain more insight into the structural details of the multilayer phase, we performed SXRD measurements using a similar Fe_3O_4 film grown *in situ* in the UHV system installed at the beamline.[31] A reciprocal space map of the Fe_3O_4/Ag(100) structure is shown in Fig. 3(a), with an inset showing the corresponding real-space unit cell. Atomic rows of Fe_3O_4 are aligned with those of the substrate, breaking the hexagonal symmetry of the structure, and for this reason, a centered-rectangular unit cell was chosen for modeling. Measurement of the in-plane diffraction angles for the Fe_3O_4 rods yields unit cell dimensions of 3.13 Å and 5.45 Å, giving a mean in-plane Fe–Fe distance of 3.14 Å, consistent with STM and LEED measurements. This lattice constant is contracted relative to monolayer FeO/Ag(100) (~3.25 Å), but expanded by about 3% relative to bulk wüstite $Fe_{1-x}O$ (3.04 Å)[2]. The in-plane width of the rods indicates island diameters in the range of 15–20 nm.

Out-of-plane SXRD scans measured along two of the Fe_3O_4 diffraction rods are plotted in Figs. 3(b) and 3(c). The essential features of the film structure can be deduced by the comparison of these curves with the calculated structure factors for simple models composed of close-packed layers of Fe atoms only, plotted together in the same panels. The major features of the XRD patterns are dominated by scattering from Fe due to its larger atomic number. The patterns of maxima and minima in the measured curves correspond well to those of the 3-layer Fe film with *fcc* stacking and rule out structures with *hcp* stacking.

From this qualitative comparison, the measurements appear to support a rocksalt model based on wüstite FeO, which exhibits the same cubic stacking in the Fe sublattice seen here. However, a significant discrepancy is apparent if we consider the layer spacing implied by the diffraction patterns. The simulated structure factors in Figs. 3(b) and 3(c) were calculated assuming a layer spacing corresponding to FeO, 2.5 Å. The experimental curves are contracted in reciprocal space by about 15%, implying a corresponding 15% expansion in the layer spacing, to about 2.9 Å [dashed lines and arrows in Figs. 3(b) and 3(c)]. If the octahedral stacking of the rocksalt phase were maintained, this would imply a significant increase in Fe–O bond length to about 2.3 Å average. For reference, bond lengths in bulk iron oxides (FeO, Fe_3O_4, α-Fe_2O_3) range from 1.88 Å (Fe_{tet} in Fe_3O_4) to 2.16 Å (Fe_{oct} in FeO), with shorter bonds generally observed for the oxides containing Fe^{3+}.[51–53] The assumption of a rocksalt structure for the film thus implies the presence of anomalously long Fe–O bonds, with no obvious physical cause.

A more reasonable explanation for the large interlayer distance is a change in coordination geometry. A change from octahedral stacking in the dense rocksalt structure to tetrahedral stacking in the more open zinc blende structure would result in an increase in the linear dimension of 15.5%, assuming fixed bond lengths. Consistent with this, models of the Fe_3O_4 film with tetrahedral coordination and the lattice parameters determined by SXRD exhibit Fe–O bond lengths in the range of 1.9–2.1 Å, consistent with expectations based on other iron oxide phases. Although the zinc blende and wurtzite structures are not stable bulk phases for FeO, there is some precedent for the formation of tetrahedral Fe in close-packed layers. A study of relatively thick films of FeO(111)[54] showed that Fe cations at the surface adopt tetrahedral coordination, produced by the introduction of a stacking fault. A similar stacking fault and change to tetrahedral coordination were observed for CoO(111).[55] Given the very small thickness of the Fe_3O_4 sheets studied here, it appears plausible that tetrahedral iron should also be present.

B. Density functional theory calculations

To confirm that the Fe_3O_4 sheets incorporate Fe in tetrahedral coordination and to resolve the details of this structure, we

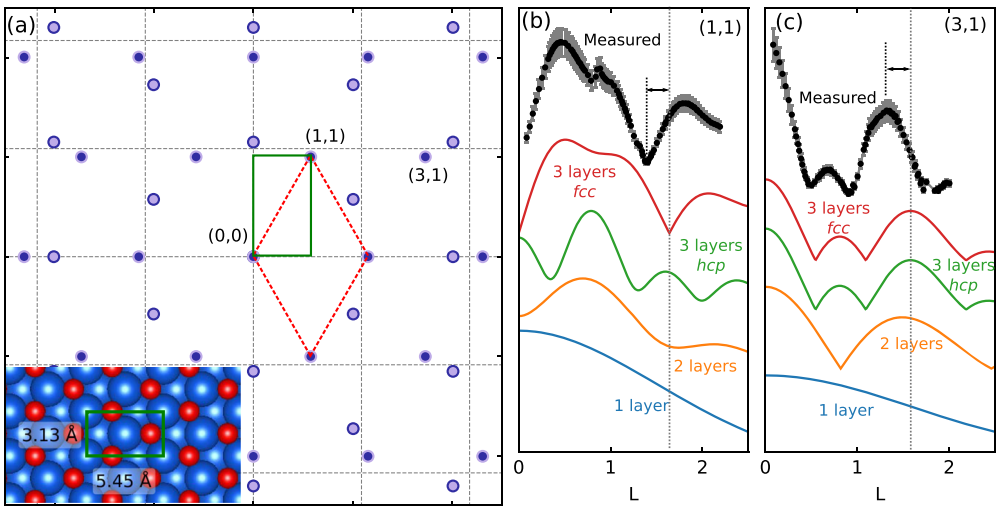

FIG. 3. (a) Reciprocal space map of the hexagonal Fe_3O_4 phase showing the positions of diffraction rods relative to the Ag(100) substrate (dashed lines). Alignment of atomic rows of the oxide with those of the substrate results in four inequivalent domains that produce two sets of non-overlapping rods. Inset shows the centered-rectangular unit cell corresponding to that in the reciprocal space map. The reciprocal-space unit cells marked here correspond to those indicated in the atomic-scale STM image in Fig. 1(a). [(b) and (c)] Measured structure factors for the (1,1) and (3,1) rods, respectively, along with calculated structure factors for simplified models consisting of close-packed sheets of Fe, with layer spacing corresponding to that in FeO(111), 2.48 Å. The dashed lines indicate the discrepancy between the measured positions of the primary maxima/minima and those expected for 3 layers of bulklike FeO.

performed a set of density functional theory calculations for different structural models within the DFT+U framework.[43] The films are shown experimentally to exhibit a fully incommensurate interface with the silver substrate, resulting in a large (approximately 16 × 12) moiré-type supercell that is too computationally demanding to treat explicitly. Therefore, as a first approximation, we modeled the films as free-standing sheets in slab supercell geometry. The DFT+U approach has been used widely in computational studies of bulk iron oxides and ultrathin films in recent years[56–58] and is a reasonable approximation for these systems.[59] Several structures were chosen for investigation, which incorporate 3 close-packed layers of iron in *fcc* stacking and 4 layers of oxygen, placed in different arrangements to yield phases with different combinations of octahedral ("O") and tetrahedral ("T") coordination. The most relevant phases are shown in Fig. 4(a). These include the purely octahedral and tetrahedral phases based on rocksalt and zinc blende lattices, as well as two hybrid structures incorporating two tetrahedral layers and one octahedral layer.

The stabilities of the most relevant phases, according to DFT+U calculations, are shown in Fig. 4(b), where total energy has been computed as a function of the in-plane lattice parameter. The zinc blende structure in which all Fe atoms are tetrahedrally coordinated (resulting in a polar configuration with dangling, singly coordinated O atoms) is found to be much higher in energy (+2.43 eV/Fe_3O_4) and is therefore omitted from the plot, as is the TTO phase, which was unstable and converged to a TOO geometry (with a *hcp*-stacked Fe lattice). The only structures found to be plausible candidates were the rocksalt phase and the TOT phase, which is a symmetrical structure incorporating an octahedral layer of Fe at the center and tetrahedral layers at the surfaces. The TOT configuration is found to be the most stable overall, about 0.27 eV/Fe_3O_4 lower than the rocksalt phase. The calculated interlayer distance for the relaxed structure is 2.91 Å, which is in good agreement with the dimensions deduced from SXRD. The calculated in-plane lattice parameter for the TOT phase is larger than what is observed experimentally by about 2%. We attribute this discrepancy to the tendency of the PBE functional to overestimate lattice constants by 1%–3%.[60] The Fe–O bond lengths are between 1.89 Å and 1.91 Å for Fe_{tet} and between 2.10 Å and 2.18 Å for Fe_{oct}, which is consistent with reference data. The calculation predicts a slight breaking of octahedral symmetry at these sites such that two Fe–O bonds are elongated with respect to the other four, resulting in approximate D_{4h} symmetry locally. It is not clear whether this is a real effect or an artifact of the unit cell and spin configuration. Depending on the exact placement of the outermost oxygen layers with respect to the inner Fe and O layers, which can resemble coordination in either wurtzite or

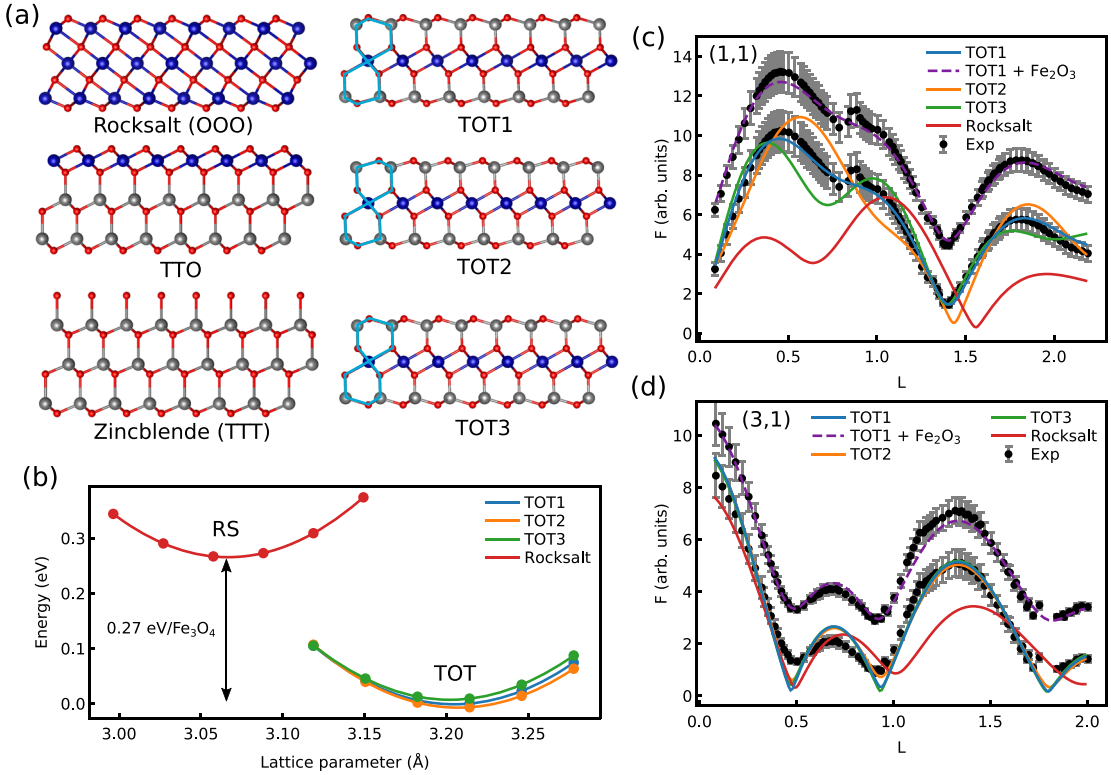

FIG. 4. (a) Structures investigated by DFT+U that are based on *fcc* iron stacking and close-packed oxygen layers. Depending on the oxygen stacking sequence, various combinations of octahedral (O) and tetrahedral (T) metal coordination are present. The rocksalt and TOT phases were found to be significantly more stable than the others. (b) Calculated energy for various phases as functions of the in-plane lattice parameter. [(c) and (d)] Structure factors calculated for the three different TOT models and for the rocksalt model using coordinates from DFT calculations. Curves are fitted to the experimental data by varying only the intensity and Debye–Waller parameter. Also plotted is the result of a fit where a minority contribution from a 2-layer Fe_2O_3 phase is added to that of the TOT1 phase (offset for clarity).

zinc blende, three different TOT structures are possible, but these are found to be very similar in energy. We denote as TOT2 the structure with zinc blende-like stacking, TOT3 the structure with wurtzite-like stacking, and TOT1 the structure incorporating both. Models of the three structures are shown in Fig. 4(a), with the difference in oxygen layer placement highlighted.

In Figs. 4(c) and 4(d), we plot the experimental x-ray rod profiles with simulated curves for the TOT and rocksalt phases, with structures determined from DFT+U. The simulation for the TOT1 phase is found to be in essentially perfect agreement with the experiment. The TOT2 and TOT3 phases are slightly worse, with residuals exceeding 10% of intensity assumed to be the uncertainty in the measurement. For the rocksalt structure, agreement with the experiment is very poor, both in terms of the positions of the minima/maxima, linked to the interlayer spacing, and the shape of the (1,1) rod for L < 1.5, the details of which are related to the positions of the oxygen layers. The very good agreement of the calculation for the TOT phases with the experiment, as well as their predicted stability, leads us to conclude that this structure is present in the experiments. The largest discrepancy between the measured and fitted rod profiles is found near the minima of the (3,1) rod at L = 0.5 and L = 0.9. We attribute this to the presence of the 2-layer Fe_2O_3 phase discussed above. As shown in Fig. 3(c), a 2-layer structure exhibits a minimum in this rod between those of the corresponding 3-layer phase so that the magnitude of the oscillation in the apparent structure factor is reduced in this range. This was verified by fitting the experimental data with the summed contributions of the TOT1 DFT structure and a Fe_2O_3 structure, with the relative contribution and the Fe–Fe interlayer spacing of the secondary phase as variable parameters. The result of this fit, which used a mixed octahedral/tetrahedral coordination similar to the TOT phase, is plotted in Figs. 4(c) and 4(d). The fit indicates a proportion of the 2-layer phase of about 20% and an interlayer spacing of 2.75 ± 0.1 Å. Due to the relatively small contribution of this phase to the overall diffraction signal, however, we do not believe that we can draw clear conclusions about its structure.

Among the three TOT phases, TOT1 clearly shows the best agreement with experiment, but due to the similarity in energy and the fairly close reproduction of experimental diffraction intensities by the TOT2 and TOT3 structures, we cannot exclude these with confidence. We note further that a combination of these phases might be formed, given the similarity in energy. In any case, calculations indicate that the effect of the difference in stacking, which does not affect local coordination environments, on properties is small. Ball models of the TOT1 Fe_3O_4 that best fits the experimental data are shown in Fig. 5.

Fe_3O_4 is formally a mixed-valence compound with a composition of $Fe^{2+}Fe_2^{3+}O_4^{2-}$. In bulk form, it crystallizes in the inverse spinel structure, with Fe^{3+} ions occupying tetrahedral sites and Fe^{2+} and Fe^{3+} ions occupying equivalent octahedral sites. Charge disproportionation and ordering are observed at low temperature and are responsible in part for the compound's complex and distinctive electronic and magnetic properties.[7] In the case of the Fe_3O_4 nanosheet considered here, the DFT+U calculations predict clear charge segregation between sites with different coordination. The Fe_{tet} exhibit more positive Bader charge (+1.66 e^- relative to an isolated, neutral Fe atom) and larger magnetic moment (4.06 μB) than the Fe_{oct} (+1.41 e^- and 3.66 μB), consistent with assignment to high-spin Fe^{3+} and Fe^{2+} states, respectively, whose charge and magnetic moments have been estimated from calculations of FeO (+1.35 e^-, 3.64–3.69 μB) and Fe_2O_3 (+1.82 e^-, 4.22 μB). Antiferromagnetic ordering, with equal numbers up and down atoms in each layer, was found to be most stable among those tested in our unit cell. Details of the investigation of charge and spin distributions will be described separately.[61]

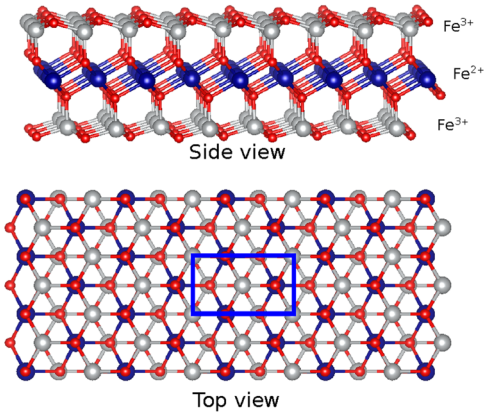

FIG. 5. Ball models of the TOT1 phase found to best reproduce the diffraction rod data. DFT+U calculations indicate that the central octahedral layer consists of Fe^{2+} while the outer tetrahedral layers are Fe^{3+}. The computational surface cell is indicated by a blue rectangle.

Figure 6 shows the total and projected densities of states calculated for the TOT1 Fe_3O_4 sheet with antiferromagnetic spin ordering. The DFT+U calculations predict a small, indirect bandgap of 0.3 eV separating filled 3*d* states on the central Fe_{oct}^{2+} sites from empty 3*d* states at the outer Fe_{tet}^{3+} sites. The smallest electronic excitations are thus predicted, at this level of theory, to involve charge transfer from the central octahedral layer to the outer tetrahedral layers.

We also performed a set of calculations of Ag-supported Fe_3O_4 sheets to test the effect of the oxide–substrate interaction and verify that the unsupported model is a good approximation. Adhesion energies, including van der Waals contributions, were computed using an Ag(100) slab with an expanded lattice parameter matching that of the Fe_3O_4 sheet. As mentioned above and discussed in Ref. 26, the real interface exhibits an incoherent moiré structure, with regions where O atom rows are in phase with those of Ag so that half are in on-top positions and regions where the O atom rows are out of phase with Ag and where half reside above fourfold hollow sites. In the rest of the structure, atoms reside above bridge and intermediate sites. Depending on the interface geometry, we find adhesion energies ranging from 0.2 eV to 0.4 eV per interface Fe/O atom (0.4–0.8 J/m^2), with the strongest bonding found where O atoms are located directly atop Ag. The adhesion energy for the real system should be intermediate between these values, as the incommensurate interface exhibits a combination of these bonding geometries. The value is significantly smaller than that calculated for iron oxide monolayers on Pt (E_{adh} > 1 eV) and is even smaller than that for FeO monolayers on Ag(100) (~0.5 eV, neglecting van der Waals corrections).[24] The calculations also show that the

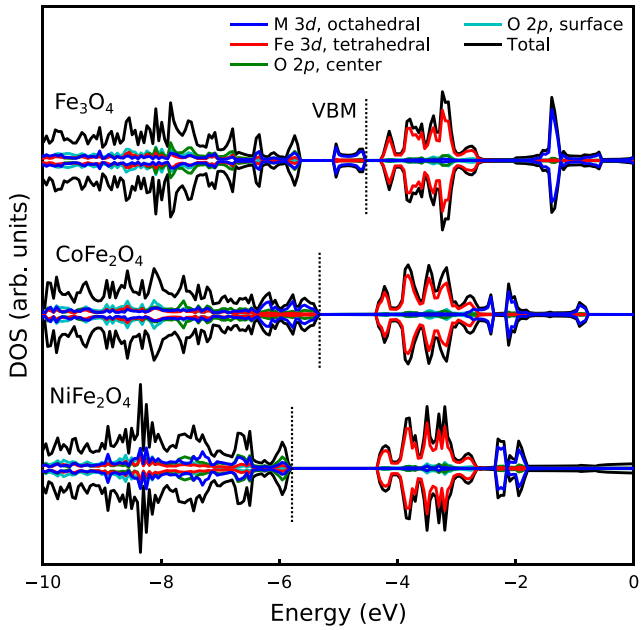

FIG. 6. Calculated total and projected densities of states for the TOT1 Fe_3O_4 structure and analogous $CoFe_2O_4$ and $NiFe_2O_4$ formed by the substitution of the central octahedral Fe layer with Co and Ni. Dashed lines mark the positions of the valence band maxima. Energies are relative to the vacuum potential.

influence of the interface on the sheet's electronic structure is minor, and Bader analysis indicates a charge transfer of only 0.1 e^- per interface O atom.

IV. DISCUSSION

Although showing similarity with bulk magnetite, in that a mix of tetrahedral and octahedral coordination states is observed in both cases, the structure of the ultrathin Fe_3O_4 phase is clearly unique. The obvious question raised by these results is whether the Fe_3O_4 sheets can be synthesized in unsupported form or whether their properties will be similar to the supported phase studied here—reasonable criteria for designation as a 2D material, as opposed to a surface oxide. Previous experiments involving FeO monolayers on Ag(100) showed that such films already interact weakly with the surface, exhibiting properties similar to those predicted for an unsupported monolayer. For such monolayers, interaction with the substrate is dominated by Ag–Fe bonds, causing the O layer to buckle outward slightly. The Fe_3O_4 sheets, on the other hand, expose an oxygen layer to the substrate and exhibit a fully incommensurate, large-period moiré coincidence structure. The calculated adhesion energy is also comparable in magnitude to what has been reported for graphene on copper.[62] Based on both the experiment and the DFT+U calculations, we conclude that the Fe_3O_4 phase interacts even more weakly with the silver surface than the monolayer and that the phase forms as a result of the inherent (meta-)stability of the configuration and not due to specific interaction with the silver surface. We therefore expect it to be stable in free-standing form as well and, aside from mechanical separation from the metal surface, could perhaps be produced by the reduction of Fe_2O_3 nanosheets.[13]

Although we cannot make strong claims regarding the nanosheets' properties at this point, these could be potentially interesting and deserve further investigation. The distinct atomic layers in the structure inherently direct charge separation, and it is expected that other metals substituted for iron as dopants should strongly favor either the central or surface layers. Noting again that the bandgap calculated for the film separates occupied states at the Fe^{2+} layer from empty states at the Fe^{3+} layer, one can hypothesize that substitution of the octahedral Fe atoms with Co or Ni, which exhibit higher third ionization energies and form more stable divalent oxides, would result in widening of the bandgap. Indeed, DFT+U calculations predict this to be the case; densities of states for $CoFe_2O_4$ and $NiFe_2O_4$ are plotted in Fig. 6. The computed bandgap is increased to 1.0 eV and 1.5 eV for the cobalt- and nickel-substituted sheets, respectively, as the occupied 3*d* states shift downward. With bandgaps in the visible range and a high surface area, these have potential for photochemical activity, for example. We speculate that it should be possible to prepare a wide variety of 2D ternary oxide phases of this type, with diverse properties that could be useful in different applications.

It is noteworthy in this context that layered double hydroxides (LDH) of iron and especially mixtures of iron and nickel are highly active electrocatalysts for the oxygen evolution reaction.[63] These LDH phases consist of single close-packed layers of metal ions in octahedral coordination to OH, and their high performance is generally linked to the inherently high surface areas provided by the 2D structure and to the favorable bonding of reaction intermediates at the metal surface sites.[64] Cai *et al.*[65] showed that NiFe LDH, ordinarily consisting of Fe^{3+} and Ni^{2+} sites, exhibit enhanced performance when synthesized with a significant portion of Fe^{2+} as well. It would be interesting, therefore, to investigate the electrocatalytic properties of the 2D Fe_3O_4 and bi/multimetallic islands, which should expose ions of different valence and coordination states at their edges.

The tetrahedral–octahedral–tetrahedral structure of the Fe_3O_4 nanosheets also suggests parallels with clays and related phyllosilicates (e.g., talc and mica), many of which exhibit a similar structure where tetrahedral silica sheets are bound together by an octahedral layer of metal ions. Variants with high concentrations of iron, both in the 2+ and 3+ states and occupying both octahedral and (to a lesser extent) tetrahedral sites, are known, and their performance as catalysts has been recognized.[66] Redox reactions involving iron in these minerals are particularly important for environmental chemistry,[67] and interestingly, it was shown recently[68] that the combination of Fe^{2+} and Fe^{3+} at the edges of 2D sheets in iron-rich clays strongly promotes their activity in oxidation reactions.

Although our investigation of the magnetic properties of the sheets was limited, the preference for antiferromagnetic ordering was clear, as mentioned above. These properties also deserve further investigation, with views toward both fundamental aspects of antiferromagnetism in 2D materials[69] and toward potential spintronics applications.[70,71]

The formation of the 2-layer Fe_2O_3 phase, not recognized in previous studies of this system, is another issue that should be addressed. It is not clear at this point whether the phase can be prepared specifically, directed by controlling the oxygen pressure, or

whether it is merely an intermediate formed in the process of conversion of the FeO bilayer to Fe_3O_4. Although, as discussed above, we cannot extract much information about this structure from the SXRD data, preliminary indications suggest that a similar mixed octahedral/tetrahedral structure is formed. We note that the two-phase fits to the diffraction rods were notably worse when a rocksalt type stacking was assumed and that the in-plane lattice parameters of the two structures are indistinguishable in our LEED and SXRD data, suggesting similar bonding configurations.

V. CONCLUSION

The structure of an ultrathin Fe_3O_4 phase grown on Ag(100) has been investigated by using SXRD and DFT+U calculations. The structure is distinct from bulk iron oxide phases and from surface oxides whose properties are defined or strongly influenced by bonding to a metal substrate. Instead, it appears to be a unique 2D material whose properties are intrinsic to its structure. Further investigations to elucidate these properties and to isolate the material in unsupported form are underway.

VI. ACKNOWLEDGMENTS

We are grateful to Matthew Forster, Jonathan Rawle, and Chris Nicklin for assistance with the SXRD experiments. This work was performed within the VR funded Röntgen-Ångström collaboration "Catalysis on the atomic scale" (Project No. 349-2011-6491) and the Knut and Alice Wallenberg (KAW) funded project "Atomistic design of new catalysts" (Project No. KAW 2015.0058). Additional funding was provided by the Swedish Research Council through Grant Nos. 2016-04162 (Olsson) and 2018-05374 (Merte), as well as the Crafoord Foundation and the Swedish Foundation for Strategic Research. We acknowledge Diamond Light Source for time on Beamline I07 under Proposal No. SI10342. DFT+U simulations were performed using computational resources provided by the Swedish National Infrastructure for Computing (SNIC) at the National Supercomputer Centre (NSC), Linköping University, and at the High Performance Computing Center North (HPC2N), Umeå University.

REFERENCES

[1] P. Tartaj, M. P. Morales, T. Gonzalez-Carreño, S. Veintemillas-Verdaguer, and C. J. Serna, Adv. Mater. **23**, 5243 (2011).
[2] R. Cornell and U. Schwertmann, *The Iron Oxides: Structure, Properties, Reactions, Occurences and Uses*, 2nd ed. (Wiley-VCH Verlag GmbH & Co. KGaA, 2003).
[3] Q. Qu, S. Yang, and X. Feng, Adv. Mater. **23**, 5574 (2011).
[4] L. Zhang, H. B. Wu, and X. W. D. Lou, Adv. Energy Mater. **4**, 1300958 (2014).
[5] W. Wu, Q. He, and C. Jiang, Nanoscale Res. Lett. **3**, 397 (2008).
[6] J. Yuan, A. Balk, H. Guo, Q. Fang, S. Patel, X. Zhao, T. Terlier, D. Natelson, S. Crooker, and J. Lou, Nano Lett. **19**, 3777 (2019).
[7] G. S. Parkinson, Surf. Sci. Rep. **71**, 272 (2016).
[8] H.-J. Freund and G. Pacchioni, Chem. Soc. Rev. **37**, 2224 (2008).
[9] S. Surnev, A. Fortunelli, and F. P. Netzer, Chem. Rev. **113**, 4314 (2013).
[10] G. Barcaro and A. Fortunelli, Phys. Chem. Chem. Phys. **21**, 11510 (2019).
[11] C. Tan, X. Cao, X.-J. Wu, Q. He, J. Yang, X. Zhang, J. Chen, W. Zhao, S. Han, G.-H. Nam, M. Sindoro, and H. Zhang, Chem. Rev. **117**, 6225 (2017).
[12] N. Mahmood, I. A. D. Castro, K. Pramoda, K. Khoshmanesh, S. K. Bhargava, and K. Kalantar-Zadeh, Energy Storage Mater. **16**, 455 (2019).
[13] A. P. Balan, S. Radhakrishnan, C. F. Woellner, S. K. Sinha, L. Deng, C. de los Reyes, B. M. Rao, M. Paulose, R. Neupane, A. Apte, V. Kochat, R. Vajtai, A. R. Harutyunyan, C.-W. Chu, G. Costin, D. S. Galvao, A. A. Martí, P. A. van Aken, O. K. Varghese, C. S. Tiwary, A. Malie Madom Ramaswamy Iyer, and P. M. Ajayan, Nat. Nanotechnol. **13**, 602 (2018).
[14] G. H. Vurens, M. Salmeron, and G. A. Somorjai, Surf. Sci. **201**, 129 (1988).
[15] M. Ritter, W. Ranke, and W. Weiss, Phys. Rev. B **57**, 7240 (1998).
[16] E. D. L. Rienks, N. Nilius, L. Giordano, J. Goniakowski, G. Pacchioni, M. P. Felicissimo, T. Risse, H.-P. Rust, and H.-J. Freund, Phys. Rev. B **75**, 205443 (2007).
[17] Y. Li, K. C. Adamsen, L. Lammich, J. V. Lauritsen, and S. Wendt, ACS Nano **13**, 11632 (2019).
[18] Q. Fu, W.-X. Li, Y. Yao, H. Liu, H.-Y. Su, D. Ma, X.-K. Gu, L. Chen, Z. Wang, H. Zhang, B. Wang, and X. Bao, Science **328**, 1141 (2010).
[19] Q. Fu, F. Yang, and X. Bao, Acc. Chem. Res. **46**, 1692 (2013).
[20] W. Kudernatsch, G. Peng, H. Zeuthen, Y. Bai, L. R. Merte, L. Lammich, F. Besenbacher, M. Mavrikakis, and S. Wendt, ACS Nano **9**, 7804 (2015).
[21] Z. Chen, Y. Mao, J. Chen, H. Wang, Y. Li, and P. Hu, ACS Catal. **7**, 4281 (2017).
[22] Y.-N. Sun, L. Giordano, J. Goniakowski, M. Lewandowski, Z.-H. Qin, C. Noguera, S. Shaikhutdinov, G. Pacchioni, and H.-J. Freund, Angew. Chem., Int. Ed. **49**, 4418 (2010).
[23] L. R. Merte, Y. Bai, H. Zeuthen, G. Peng, L. Lammich, F. Besenbacher, M. Mavrikakis, and S. Wendt, Surf. Sci. **652**, 261 (2016).
[24] L. R. Merte, C. J. Heard, F. Zhang, J. Choi, M. Shipilin, J. Gustafson, J. F. Weaver, H. Grönbeck, and E. Lundgren, Angew. Chem., Int. Ed. **55**, 9267 (2016).
[25] D. Bruns, I. Kiesel, S. Jentsch, S. Lindemann, C. Otte, T. Schemme, T. Kuschel, and J. Wollschläger, J. Phys.: Condens. Matter **26**, 315001 (2014).
[26] L. R. Merte, M. Shipilin, S. Ataran, S. Blomberg, C. Zhang, A. Mikkelsen, J. Gustafson, and E. Lundgren, J. Phys. Chem. C **119**, 2572 (2015).
[27] H. C. Galloway, J. J. Benitez, and M. Salmeron, Surf. Sci. **298**, 127 (1993).
[28] H. Zeuthen, W. Kudernatsch, G. Peng, L. R. Merte, L. K. Ono, L. Lammich, Y. Bai, L. C. Grabow, M. Mavrikakis, S. Wendt, and F. Besenbacher, J. Phys. Chem. C **117**, 15155 (2013).
[29] G. Ketteler and W. Ranke, J. Phys. Chem. B **107**, 4320 (2003).
[30] N. A. Khan and C. Matranga, Surf. Sci. **602**, 932 (2008).
[31] C. Nicklin, T. Arnold, J. Rawle, and A. Warne, J. Synchrotron Rad. **23**, 1245 (2016).
[32] J. Drnec, T. Zhou, S. Pintea, W. Onderwaater, E. Vlieg, G. Renaud, and R. Felici, J. Appl. Crystallogr. **47**, 365 (2014).
[33] E. Vlieg, J. Appl. Crystallogr. **30**, 532 (1997).
[34] E. Vlieg, J. Appl. Crystallogr. **33**, 401 (2000).
[35] G. Kresse and J. Hafner, Phys. Rev. B **47**, 558 (1993).
[36] G. Kresse and J. Hafner, Phys. Rev. B **49**, 14251 (1994).
[37] G. Kresse and J. Furthmüller, Comput. Mater. Sci. **6**, 15 (1996).
[38] G. Kresse and J. Furthmüller, Phys. Rev. B **54**, 11169 (1996).
[39] P. E. Blöchl, Phys. Rev. B **50**, 17953 (1994).
[40] G. Kresse and D. Joubert, Phys. Rev. B **59**, 1758 (1999).
[41] J. P. Perdew, K. Burke, and M. Ernzerhof, Phys. Rev. Lett. **77**, 3865 (1996).
[42] S. Grimme, J. Comput. Chem. **27**, 1787 (2006).
[43] S. L. Dudarev, G. A. Botton, S. Y. Savrasov, C. J. Humphreys, and A. P. Sutton, Phys. Rev. B **57**, 1505 (1998).
[44] H. Bowen, D. Adler, and B. Auker, J. Solid State Chem. **12**, 355 (1975).
[45] J. van Elp, J. L. Wieland, H. Eskes, P. Kuiper, G. A. Sawatzky, F. M. F. de Groot, and T. S. Turner, Phys. Rev. B **44**, 6090 (1991).
[46] M. Cococcioni and S. de Gironcoli, Phys. Rev. B **71**, 035105 (2005).
[47] H. J. Monkhorst and J. D. Pack, Phys. Rev. B **13**, 5188 (1976).
[48] J. Neugebauer and M. Scheffler, Phys. Rev. B **46**, 16067 (1992).
[49] R. Bader, *Atoms in Molecules: A Quantum Theory*, International Series of Monographs on Chemistry (Clarendon Press, 1994).
[50] W. Tang, E. Sanville, and G. Henkelman, J. Phys.: Condens. Matter **21**, 084204 (2009).
[51] C. Haavik, S. Stølen, H. Fjellvåg, M. Hanfland, and D. Häusermann, Am. Mineral. **85**, 514 (2000).

[52]E. N. Maslen, V. A. Streltsov, N. R. Streltsova, and N. Ishizawa, Acta Crystallogr., Sect. B: Struct. Sci. **50**, 435 (1994).
[53]H. Fjellvåg, F. Grønvold, S. Stølen, and B. Hauback, J. Solid State Chem. **124**, 52 (1996).
[54]L. Martín-García, I. Bernal-Villamil, M. Oujja, E. Carrasco, R. Gargallo-Caballero, M. Castillejo, J. F. Marco, S. Gallego, and J. de la Figuera, J. Mater. Chem. C **4**, 1850 (2016).
[55]K. Heinz and L. Hammer, J. Phys.: Condens. Matter **25**, 173001 (2013).
[56]L. Giordano, G. Pacchioni, J. Goniakowski, N. Nilius, E. D. L. Rienks, and H.-J. Freund, Phys. Rev. B **76**, 75416 (2007).
[57]L. R. Merte, L. C. Grabow, G. Peng, J. Knudsen, H. Zeuthen, W. Kudernatsch, S. Porsgaard, E. Lægsgaard, M. Mavrikakis, and F. Besenbacher, J. Phys. Chem. C **115**, 2089 (2011).
[58]Y. Ning, M. Wei, L. Yu, F. Yang, R. Chang, Z. Liu, Q. Fu, and X. Bao, J. Phys. Chem. C **119**, 27556 (2015).
[59]S. Prada, L. Giordano, G. Pacchioni, C. Noguera, and J. Goniakowski, J. Chem. Phys. **141**, 144702 (2014).
[60]P. Haas, F. Tran, and P. Blaha, Phys. Rev. B **79**, 085104 (2009).
[61]P. A. T. Olsson, L. R. Merte, and H. Grönbeck, "Stability, magnetic order and electronic properties of ultrathin Fe_3O_4 nanosheets" (Submitted).
[62]T. Yoon, W. C. Shin, T. Y. Kim, J. H. Mun, T.-S. Kim, and B. J. Cho, Nano Lett. **12**, 1448 (2012).
[63]M. Gong, Y. Li, H. Wang, Y. Liang, J. Z. Wu, J. Zhou, J. Wang, T. Regier, F. Wei, and H. Dai, J. Am. Chem. Soc. **135**, 8452 (2013).
[64]M. Gong and H. Dai, Nano Res. **8**, 23 (2015).
[65]Z. Cai, D. Zhou, M. Wang, S.-M. Bak, Y. Wu, Z. Wu, Y. Tian, X. Xiong, Y. Li, W. Liu, S. Siahrostami, Y. Kuang, X.-Q. Yang, H. Duan, Z. Feng, H. Wang, and X. Sun, Angew. Chem. **130**, 9536 (2018).
[66]E. Garrido-Ramírez, B. Theng, and M. Mora, Appl. Clay Sci. **47**, 182 (2010).
[67]T. B. Hofstetter, R. P. Schwarzenbach, and S. B. Haderlein, Environ. Sci. Technol. **37**, 519 (2003).
[68]A. G. Ilgen, R. K. Kukkadapu, K. Leung, and R. E. Washington, Environ. Sci.: Nano **6**, 1704 (2019).
[69]M. Gibertini, M. Koperski, A. F. Morpurgo, and K. S. Novoselov, Nat. Nanotechnol. **14**, 408 (2019).
[70]R. Lebrun, A. Ross, S. A. Bender, A. Qaiumzadeh, L. Baldrati, J. Cramer, A. Brataas, R. A. Duine, and M. Kläui, Nature **561**, 222 (2018).
[71]T. Jungwirth, J. Sinova, A. Manchon, X. Marti, J. Wunderlich, and C. Felser, Nat. Phys. **14**, 200 (2018).